Electrodeposition of Si from organic solvents and studies related to initial stages of Si growth

Thiruvengadam Munisamy, Allen J. Bard*

Center for Electrochemistry, Department of Chemistry and Biochemistry, The University of Texas at Austin, Austin, TX 78712, USA

ABSTRACT

Electrodeposition of Si on substrates such as Ni, Ag and GC from acetonitrile and tetrahydrofuran containing SiCl$_4$ and SiHCl$_3$ as precursors is reported. The deposits readily oxidize on exposure to air but XPS analysis of a deposit with minimum contact with air confirms that elemental Si (2p, 99.5 eV) is electrodeposited. The deposits contained C, O, N and Cl impurities; annealing under argon improved the quality of the deposits. Studies related to initial stages of Si growth using cyclic voltammetry and chronoamperometry suggest that growth occurs via four stages (1) nucleation and localized growth, (2) growth in between islands, (3) growth inhibition and (4) slow growth stage and the growth is inhibited after a layer (~2 nm) of Si is electrodeposited on the substrate.

© 2010 Elsevier Ltd. All rights reserved.

1. Introduction

We describe experiments on the electrodeposition of Si, with special interest in the eventual fabrication of thin film Si solar cells as an alternative to bulk solar cells made from expensive single crystal Si wafers. Conversion efficiencies of 9% for polycrystalline Si [1] and 15% for amorphous Si–H [2] thin film solar cells have been reported. Current techniques to manufacture Si thin films, such as chemical vapor deposition, have disadvantages in terms of cost, complex equipment design and slow rate of deposition on a large scale, so alternative methods of fabrication are of interest. Electrodeposition offers a potentially simple and low-cost means to obtain thin films of metals [3] and semiconductors [4] and electrodeposited films of materials like CuIn$_x$Ga$_{1−x}$Se$_2$ and other chalcogenides have demonstrated high efficiency in solar cell applications [5,6]. Key issues include the purity, crystallinity, stability, and photoefficiency of the deposited semiconductor. These are functions of the solvent, precursors, current density, and substrate material.

There have been previous reports on the electrodeposition of Si from organic solvents using SiX$_4$ and SiHX$_3$ (X = Cl, Br) as precursors. Electrodeposition of Si must be performed under an inert atmosphere in organic solvents because the precursors react with moisture rapidly to form oxides (Eq. (1)) and Si is deposited at

negative potentials

$$SiX_4 + 2H_2O \rightarrow SiOX_3 + HX \text{ to } SiO_2 + 4HX \qquad (1)$$

beyond the background reduction of water. Agrawal and Austin [7] reported Si electrodeposition from propylene carbonate using SiHCl$_3$ as the precursor. Si films of 1 to 3 μm thickness were deposited on substrates such as Pt, Ti, Ti–6Al–4V alloy, n-Si and ITO coated fused silica at different temperatures ranging from 35 to 145 °C. The deposits contained roughly 3% SiO with traces of metal impurities and some Si in the form of Si–H$_2$ or Si–H. The authors stated that uniform and smooth deposits were obtained at high temperature, high precursor concentration and with a small cation supporting electrolyte. Gobet and Tannenberger [8] reported Si electrodeposition from tetrahydrofuran (THF) using SiHCl$_3$, SiCl$_4$ and SiBr$_4$ as precursors. Si films of 0.25 μm thickness were deposited on Pt, Au, Ni, Cu, GC and ITO glass substrates. Deposits contained C (~8 at.%), O (~8 at.%) and Cl (~1.5 at.%) as impurities. The authors raised an important question on whether the deposit oxidized in situ during electrodeposition in the glove box or on contact with the atmosphere. Nicholson [9] reported comprehensive work on Si electrodeposition from propylene carbonate and THF using SiCl$_4$ and SiBr$_4$ as precursors. Si was electrodeposited on n-type Si and Ti substrates. Carbon, oxygen, hydrogen and chlorine atoms were present as impurities in the deposits. Deposits had a honeycombed or reticulated morphology and oxidized on exposure to air (or even in the glove box). The work also reported a heterojunction solar cell made from electrodeposited Si with a conversion efficiency of 1.8%. Nishimura and Fukunaka [10] electrodeposited Si from propylene carbonate using SiCl$_4$ as the precursor on a nickel

substrate. The authors reported a Si deposit of 50 μm thickness with O and Cl impurities and the deposit oxidized rapidly on contact with air. The 50 μm thick deposit most likely contained propylene carbonate and tetrabutylammonium chloride breakdown products because the deposition was carried out at a potential where solvent and supporting electrolyte decomposition occurred.

Si is a semiconductor and when intrinsic behaves as an insulator. It can be doped with group 13 and 15 elements to form p-type and n-type materials, respectively, with a much higher conductivity. Crystalline Si with unprotected Si bonds easily oxidizes forming SiO_2 on the surface. The electrodeposition of Si is challenging because of the insulating nature of intrinsic Si; the deposition also needs to be carried out at a very negative potential and it is difficult to get a good deposit free of bath impurities. A stable Si film with good photovoltaic characteristics and mechanistic information about the process has not been reported. In this study, attempts were made to electrodeposit a stable Si film from acetonitrile and THF using $SiCl_4$ and $SiHCl_3$ as precursors and to study the initial stages of Si growth during electrodeposition in organic solvents.

2. Experimental

2.1. Materials

Solvents acetonitrile (CH_3CN) and tetrahydrofuran (THF) purchased from Fisher Scientific (Fair Lawn, NJ) were distilled under nitrogen from calcium hydride and sodium benzophenone, respectively. In some cases, CH_3CN (puriss, $H_2O \leq 10$ ppm) purchased from Aldrich (Allentown, PA) and THF (anhydrous, $H_2O < 50$ ppm) purchased from Acros Organics (Bridgewater, NJ) were used as received. Tetrabutylammonium chloride (TBACl, puriss, $\geq 99\%$) was purchased from Fluka (Allentown, PA) and vacuum dried at $100\,^{\circ}C$. Si tetrachloride ($SiCl_4$, 99.998%) purchased from Aldrich (Milwaukee, WI) and trichlorosilane ($SiHCl_3$, 98%) purchased from Alfa Aesar (Ward Hill, MA) were used as received. Foils of Ni, Ag, glassy carbon (GC), Pt, Au and Sn were purchased from Alfa Aesar (Ward Hill, MA), cleaned with different grades (1, 0.3, 0.05 μm) of alumina, sonicated in deionized water and rinsed with acetone prior to electrodeposition experiments.

2.2. Instrumentation

All experiments were carried out in a helium-atmosphere glove box (Vacuum Atmospheres Corp.). A CH Instruments Electrochemical Workstation (model 660) was used for electrochemical experiments. For cyclic voltammetry and chronoamperometry experiments, a 2 mm Pt disk, a Pt foil and a silver wire were used as the working, counter and quasi-reference (QRE) electrodes, respectively. KIMTECH science Kimwipes was used to clean the working electrode after each run. For electrodeposition experiments, a 1 cm^2 foil (Ni, Ag, or GC), a 1 cm^2 Pt foil and a Pt or Ag wire were used as the working, counter and quasi-reference electrodes, respectively. A single compartment cylindrical glass cell (6 cm (height) × 1.3 cm (radius)) was used for electrodeposition experiments. Metal wire QREs were employed to eliminate the possibility of contamination of the solution from the reference electrode. Since chloride ion was included in the electrolyte, the potential of the Ag wire was reasonably stable, typically the measured potential vs. the QRE was the same within ±0.04 V.

XPS spectra were recorded with an X-ray photoelectron spectrometer (Kratos Axis Ultra), utilizing a monochromated Al–Kα X-ray source ($h_n = 1486.5$ eV), hybrid optics (employing a magnetic and electrostatic lens simultaneously) and a multi-channel plate and delay line detector coupled to a hemispherical analyzer. All spectra were recorded using an aperture slot of 300 μm × 700 μm,

and high resolution spectra were collected with pass energy of 20 eV. The pressure in the analysis chamber was typically 2×10^{-9} Torr during data acquisition. Kratos XPS analysis software was used to determine the stoichiometry of samples from corrected peak areas and employing sensitivity factors for each element of interest. All binding energies were referenced to C 1s (284.5 eV) binding energy for data analysis.

SEM images were taken using a thermally assisted field emission SEM (model LEO 1530) equipped with an in-lens detector and elemental composition analysis was carried out using an energy dispersive X-ray (EDS) detector. Typical electron beam settings were a 10 kV beam voltage and an extraction current of 130 μA. A Bruker-Nonius D8 advance powder diffractometer was used for X-ray diffraction measurements.

3. Results

3.1. Electrodeposition studies

Si was electrodeposited on Ni, Ag, GC, Pt and Au substrates from two baths (1) 0.3 M $SiCl_4$, 0.1 M TBACl and CH_3CN and (2) 0.3 M $SiHCl_3$, 0.1 M TBACl and THF. Electrodeposition from the $SiCl_4$ bath was carried out in controlled potential mode (deposition potential: −2.4 V vs. Pt QRE). Deposits of about 0.5–1 μm in thickness (calculated assuming a charge passed, $n = 4$, 100% current efficiency and a density of 2.2 g/cm^3) were obtained from the $SiCl_4$ bath. Deposits were amorphous and oxidized on contact with air forming SiO_2 (deposits were brownish yellow in the glove box and turned white on contact with air over a period of several hours). XPS analysis showed the presence of C, O, N and Cl impurities. The morphology of the deposit varied depending upon type of substrate and supporting electrolyte employed. For example, the deposit on glassy carbon was nodular with few cracks (Fig. 1a), on Ni, it was agglomerate (Fig. 1b) and on Pt, it was non-uniform consisting of small plate-like structures (Fig. 1c).

To determine whether pure Si is electrodeposited, Si was deposited on a Ni substrate from a $SiCl_4$ bath. The sample was rinsed in CH_3CN and transferred to the XPS chamber using a device (Kratos WG-357) that is designed to take in a sample in the glove box, place it in a mobile vacuum desiccator, and then connect it to the XPS without exposure to the atmosphere. In this way, the sample contact with air was minimized (but not completely eliminated due to difficulty in making the connection to the XPS without the allowance of some small leakage). The sample analyzed after 2 h of evacuation in the XPS chamber showed two Si 2p peaks: a peak at 99.5 eV for Si and a peak at 103.3 eV for SiO_2 (Fig. 2a) indicating that a mixture of pure and oxidized forms of Si were present in the deposit. Etching of the deposit (with an Ar$^+$ beam) resulted in a progressive increase of Si atomic concentration and decrease of oxygen atomic concentration (Fig. 2b). The atomic concentration of C decreased and Cl first increased and then decreased. Traces of nitrogen (2 at.%) were also present in the deposit. At the end of the etch cycles, the two Si 2p peaks coalesced to form a broad peak at 101.14 eV. The formation of a broad peak with binding energy greater than 99.5 eV was also observed when a p-type Si{100} wafer was etched and is due to incorporation of Ar$^+$ ion in the deposit, formation of SiC and mixing of SiO_x during etching [11]. Thus XPS analysis of a deposit with minimum contact with air confirms that pure Si is electrodeposited and that elements from solvent and supporting electrolyte get trapped in the deposit. Oxidation of the deposit might have occurred while loading the sample from the air sensitive transport device to the XPS chamber.

Electrodeposition from $SiHCl_3$ baths was carried out at controlled potential (deposition potential: −2.0 V vs. Pt). The deposits ~0.2–0.4 μm thickness were amorphous and oxidized on contact with air. Oxidation of deposits obtained from the $SiHCl_3$ bath was
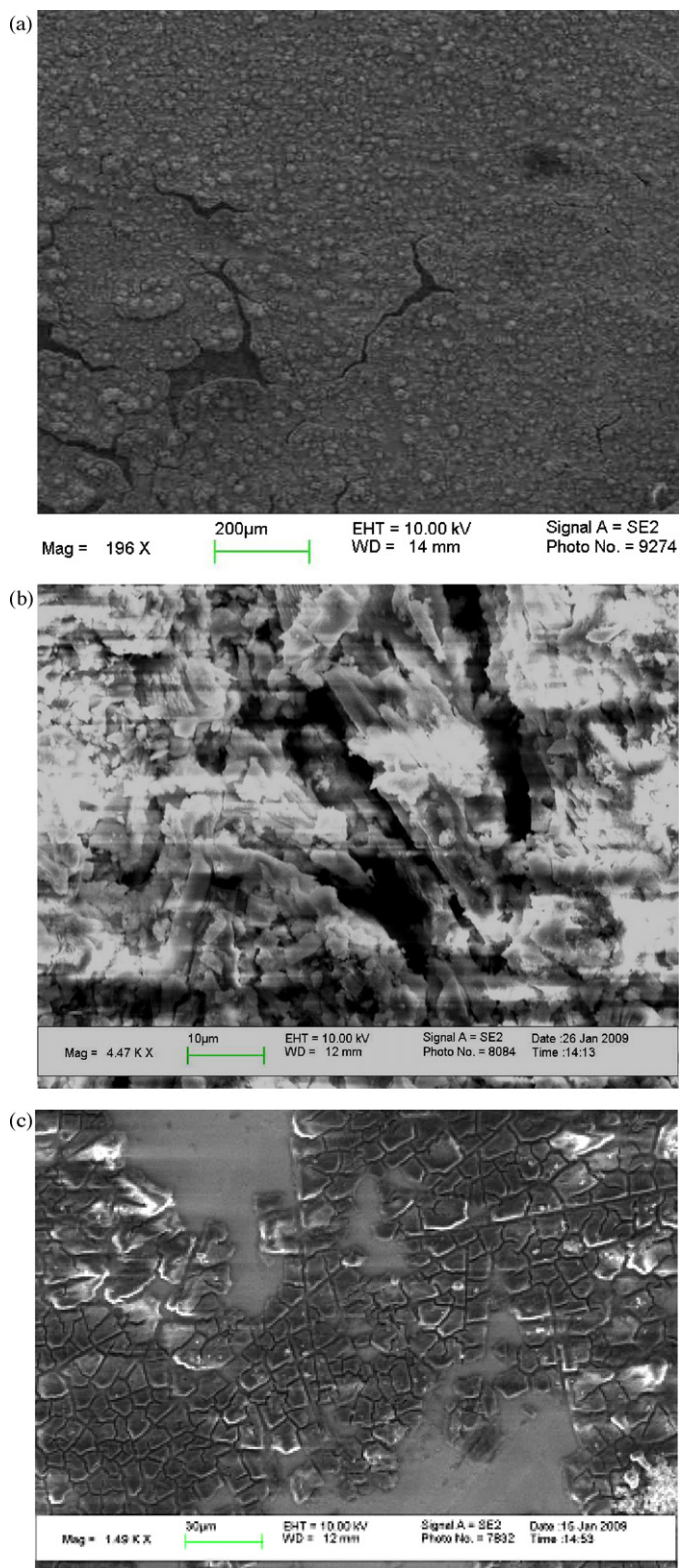
(a)

200μm
Mag = 196 X   EHT = 10.00 kV   Signal A = SE2
                     WD = 14 mm   Photo No. = 9274

(b)

10μm
Mag = 4.47 K X   EHT = 10.00 kV   Signal A = SE2   Date :26 Jan 2009
                     WD = 12 mm   Photo No. = 8084   Time :14:13

(c)

30μm
Mag = 1.49 K X   EHT = 10.00 kV   Signal A = SE2   Date :16 Jan 2009
                     WD = 12 mm   Photo No. = 7832   Time :14:53

Fig. 1. (a) Si deposit on a glassy carbon substrate. (b) Si deposit on a nickel substrate. (c) Si deposit on a platinum substrate.

slower than deposits from the $SiCl_4$ bath because of H-termination of Si bonds [7]. The deposits contained C, O, N and Cl impurities (Fig. 3a). The deposits obtained from the $SiHCl_3$ bath were then transferred to a tube furnace under an argon blanket and annealed under argon to remove excess hydrogen and bath impurities and to stabilize the film [12]. Annealing temperatures ranging from 350 to

800 °C showed a reduced presence of oxygen in the deposit (1:1 at.% ratio of Si to O in annealed samples compared to 1:2 ratio of Si:O in non-annealed samples, from EDS) and the presence of no or a low concentration of C, N and Cl impurities (Fig. 3b).

In one such annealing case, a Si–H deposit (0.17 μm) on a silver substrate from a bath containing 0.3 M $SiHCl_3$, 0.1 M TBACl, 5 mM $AlCl_3$ (a p-type dopant) and THF was annealed at 350 °C for 30 min under an argon atmosphere. Accidental presence of solder on the electrode surface (Kester, rosin core, Sn 60%/Pb 40%, melting range: 183–190 °C), which was used to make electrical contact between the silver substrate and copper wire, appeared to induce crystallization of Si. A thin layer of metals such as Ag, Ni, Sn and Al are known to induce crystallization of amorphous Si–H to form polycrystalline Si at low temperatures [13,14]. Since the solder has a low melting point and high diffusivity, it might also induce the crystallization of a-Si–H. Analysis of the sample with SEM showed isolated crystals (Fig. 4a) and EDS at these spots showed the presence of 91 at.% Si and 9 at.% aluminum. XRD analysis of the sample showed peaks due to Si{1 1 1}, Sn, Pb and some unknown peaks. The sample exhibited very small p-type photoactivity, i.e. when the sample was irradiated with a Xenon lamp, a positive shift of 16 mV in the open circuit potential resulted (Fig. 4b). Experiments with purposeful addition of solder on silver substrates followed by a-Si–H electrodeposition and annealing at 350 °C for 30 min showed similar results. More controlled studies involving slow diffusion of metal during annealing and electrodeposition of a thin layer of Si is necessary to further explore these results.

3.2. Other electrodeposition results

Electrodeposition from CH_3CN using $SiBr_4$ and SiI_4 as precursors was carried out and deposits oxidized as usual on contact with air.
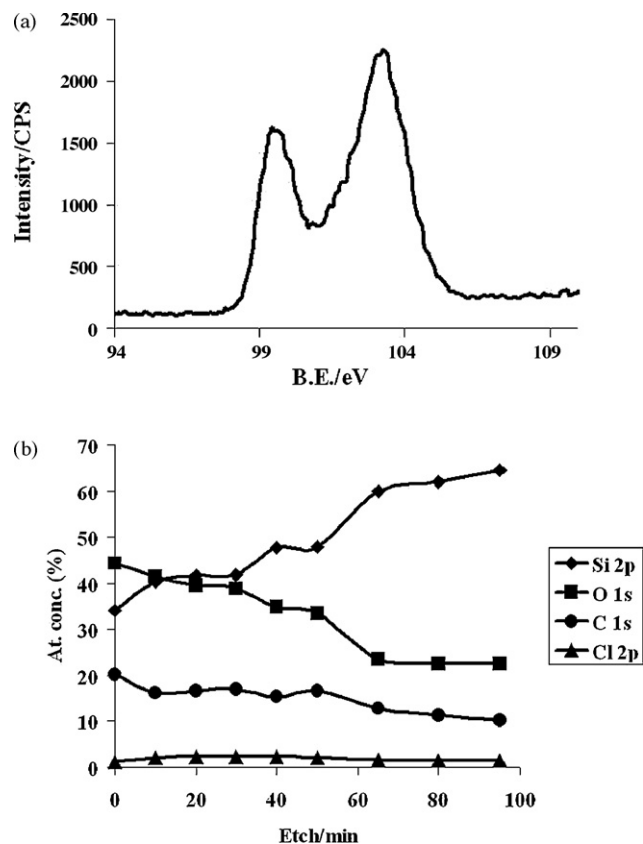
(a)

(b)

Fig. 2. (a) XPS of a Si deposit with minimum contact with air. Si 2p region: 99.5 eV (Si) and 103.3 eV (SiO_2). (b) Etching of Si deposit with Ar⁺ beam. Variation of at. conc. of Si, O, C, Cl as a function of etching time.
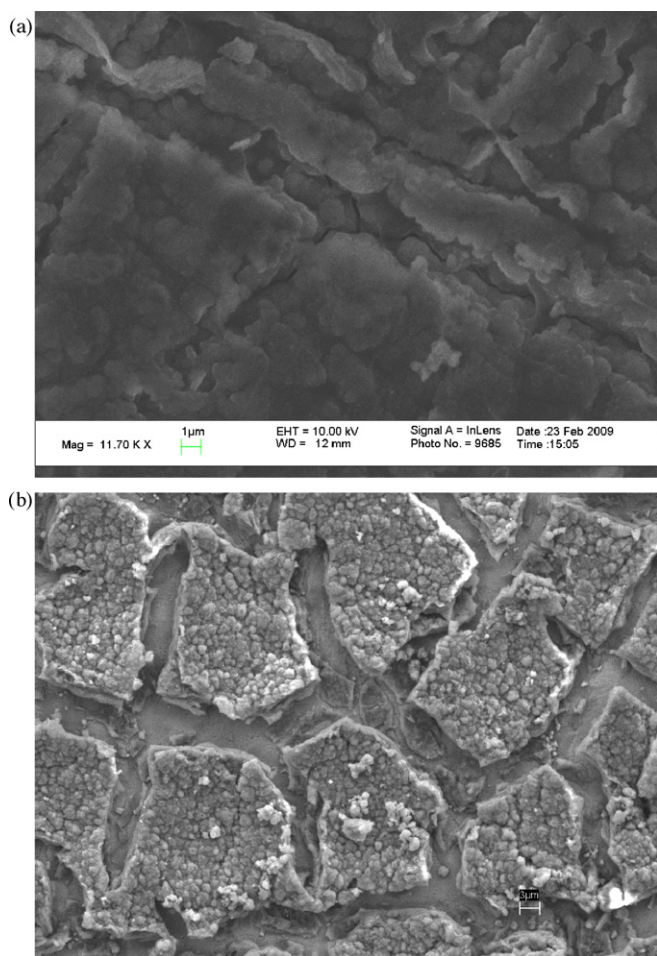
Fig. 3. (a) Si–H deposit on a nickel substrate. EDS: Si (19 at.%), O (36 at.%), C (35 at.%), N (9 at.%) and Cl (1 at.%). (b) Si–H deposit on a nickel substrate after annealing at 500 °C for 2 h. EDS: Si (44 at.%), O (55 at.%) and Cl (1 at.%).

The SiBr$_4$ and SiI$_4$ baths were less stable (a color change from transparent to yellow was observed) compared to SiCl$_4$ and SiHCl$_3$ baths [8]. Electrodeposition from SiCl$_4$ baths in the presence of triethylamine (as a H$^+$ scavenger) and at a higher temperature (~70 °C) showed no improvement in the quality of the deposit. Electrodeposition (SiCl$_4$ bath) with a pool of mercury as the substrate formed an unstable flimsy material and EDS analysis confirmed it to be Si. Co-deposition of Si and tin resulted in preferential deposition of tin, but in the case of Si and Al, Si was deposited. EDS analysis of Si deposits prepared with aluminum as the dopant consistently showed a reduced presence of oxygen (Si ~33 at.%, O ~27 at.%, C ~38 at.%, Cl ~1 at.% and Al ~1 at.%), which agrees with an observation by Nicholson of an improved deposit with the use of leveling agents [9].

3.3. Cyclic voltammetry and chronoamperometry studies

The fundamentals of SiHCl$_3$ reduction and the electrodeposition in MeCN were studied using CV and chronoamperometric techniques. A cyclic voltammogram obtained using a 0.5 mm diameter Pt disk electrode from a solution of 10 mM SiHCl$_3$, 0.1 M TBACl and CH$_3$CN showed two irreversible reduction peaks (Fig. 5a): a wave at −0.80 V vs. Ag QRE for H$^+$ reduction and a peak at −1.50 V for SiHCl$_3$ reduction. The large H$^+$ wave results from the reaction of traces of water (from the solvent and supporting electrolyte) with SiHCl$_3$ producing HCl (Eq. (1)). Note that the rather sharp peak current for SiHCl$_3$ reduction does not represent a diffusion limited cur-

rent, but rather the blocking of the electrode by a resistive film that forms as Si–H is electrodeposited on the electrode. The second cycle showed complete absence of the H$^+$ reduction wave and a considerably diminished SiHCl$_3$ reduction current (about 30% of the first cycle peak current). Agrawal and Austin [7] and Gobet and Tannenberger [8] reported similar CV results. Although Agrawal et al. suggested that the absence of H$^+$ reduction in the second cycle was due to depletion of H$^+$ after the first cycle [7], a blocking effect by the Si–H is more likely. A clean Pt electrode cycling only in the H$^+$ reduction region in this solution showed an H$^+$ reduction peak during the second and third cycles. Proton reduction on Pt is an inner-sphere heterogeneous electron transfer process and requires active Pt sites. When the Pt electrode surface is covered with Si–H at the end of the first cycle, these active sites are blocked, resulting in the total inhibition of H$^+$ reduction during the subsequent cycles. The high blockage of H$^+$ reduction suggests that most of the Pt surface is blocked and that this reaction does not occur on Si–H. On the other hand, some SiHCl$_3$ reduction continues on the second cycle. The low reduction current and wave-like feature for SiHCl$_3$ reduction on the second cycle suggests that this reduction occurs through defects (cracks and pinholes) behaving as isolated ultra-microelectrodes. The current in this region continues to decrease on subsequent scans, but is still perceptible after five cycles.

A cyclic voltammogram (Fig. 5b) obtained from a solution of 15 mM SiCl$_4$, 0.1 M TBACl and CH$_3$CN using a 2 mm Pt electrode showed similar characteristics as the SiHCl$_3$ system: an irreversible reduction peak at −0.60 V vs. Ag QRE for H$^+$ reduction and an irreversible reduction peak at −1.60 V for SiCl$_4$ reduction. During the
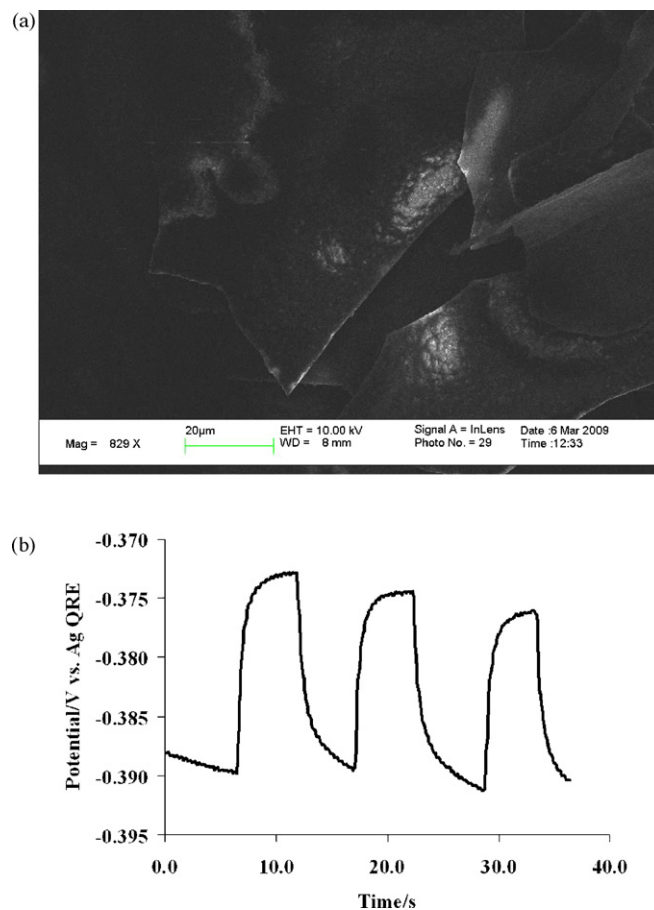

Fig. 4. (a) SEM image of Si crystals obtained by annealing of an amorphous Si–H deposit in the presence of a Sn/Pb metal mixture at 350 °C for 30 min. EDS: Si (91 at.%) and Al (9 at.%). (b) Open circuit potential variation with light, 1 mM ethyl viologen, 0.1 M TBACl and CH$_3$CN.

second cycle, H⁺ reduction was again completely inhibited and a wave-shaped reduction current for SiCl₄ with a maximum current of 40% of first cycle peak current was observed. Third and fourth CV cycles showed similar characteristic wave-shaped reduction currents for SiCl₄ reduction. A cyclic voltammogram obtained from a 6 mM SiCl₄ solution using a 25 μm diameter Pt ultramicroelectrode at a scan rate of 0.020 V/s showed a transient response (peak-shaped) rather than a steady state (wave-shaped) response due to deposition of Si on the Pt electrode surface, thereby confirming that mass transfer limitation is never reached. An interesting feature observed in the cyclic voltammograms of SiHCl₃ and SiCl₄ is that the start of the reduction current becomes less negative during the second and third cycles.

Chronoamperometry experiments were carried out to study the initial stages of Si growth. A chronoamperogram obtained from a 15 mM SiHCl₃ solution using a 2 mm Pt electrode is shown in Fig. 6a and b. The chronoamperogram has four characteristic regions: an initial transient current region (A, 1–25 ms), a steady state current region (B, 25–250 ms), an exponential decay current region (C, 250 ms to 3.5 s) and a final semi-steady state current region (D, 3.5–10 s). The capacitive charging current time constant ($R_u C_d$) for the system, obtained from a potential step from 0.47 to 0.52 V vs. Ag QRE was 0.1 ms and the current measurement shown in Fig. 6a starts at 1 ms, well after double layer charging. Qualitatively we assign the initial transient current region to nucleation and localized growth of Si (Si–H) on Pt, the steady state current region to growth in the regions between Si islands, and the exponential decay current region to formation of a mostly complete Si layer on Pt (~2 nm) and growth inhibition. The final semi-steady state current region probably corresponds to slow growth of Si by diffusion of SiHCl₃ through defects (cracks and pinholes). The deposit perhaps undergoes structural rearrangements to sustain semi-steady state growth as seen in longer chronoamperometry experiments. Exper-
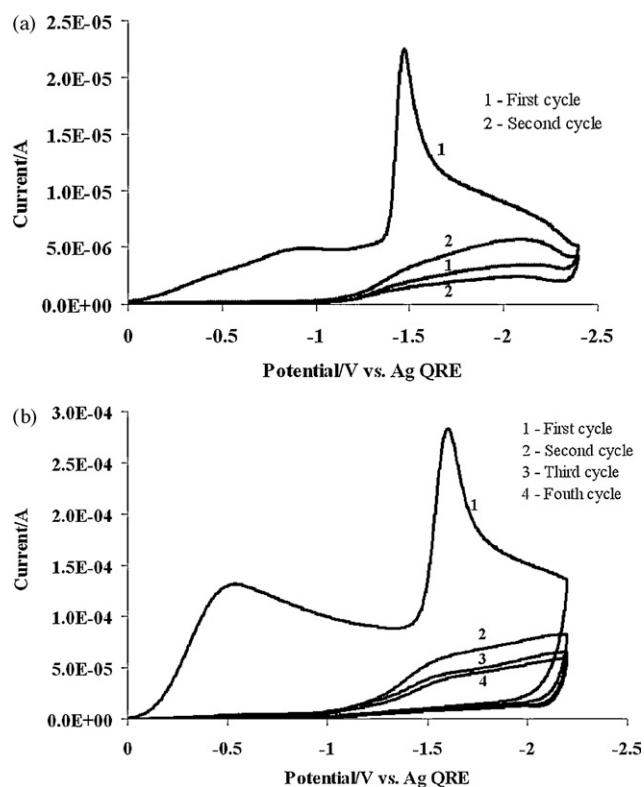

(a) Chronoamperogram of 15 mM SiHCl₃ in 0.1 M TBACl and CH₃CN. W.E. 2 mm Pt. $E_i = 0$ V vs. Ag QRE, $E_f = -1.53$ V vs. Ag QRE. (b) I vs. t plot of (a).
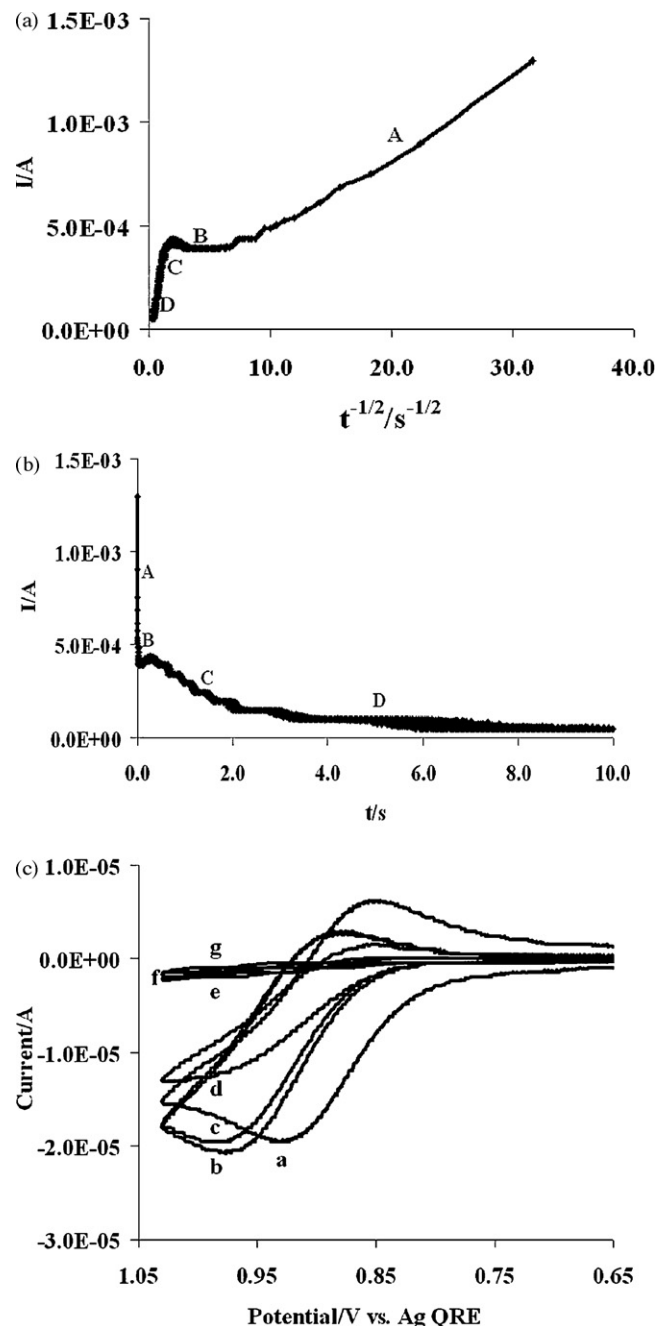

Fig. 6. (a) Chronoamperogram of 15 mM SiHCl₃ in 0.1 M TBACl and CH₃CN. W.E. 2 mm Pt. $E_i = 0$ V vs. Ag QRE, $E_f = -1.53$ V vs. Ag QRE. (b) I vs. t plot of (a). (c) Cyclic voltammograms of 1 mM ferrocene in 0.1 M TBACl and CH₃CN using Si–H deposited Pt electrodes: a, 2 mm Pt electrode; b, Si–H deposited Pt (1 ms, 13 μC/cm²); c, Si–H deposited Pt (10 ms, 51 μC/cm²); d, Si–H deposited Pt (250 ms, 668 μC/cm²); e, Si–H deposited Pt (1000 ms, 3503 μC/cm²); f, Si–H deposited Pt (3000 ms, 4745 μC/cm²); g, Si–H deposited Pt (5000 ms, 5382 μC/cm²).

Fig. 5. (a) Cyclic voltammogram of 10 mM SiHCl₃ in 0.1 M TBACl and CH₃CN. W.E. 0.5 mm Pt, $\nu = 0.2$ V/s. (b) Cyclic voltammogram of 15 mM SiCl₄ in 0.1 M TBACl and CH₃CN. W.E. 2 mm Pt, $\nu = 0.2$ V/s.

iments with 2 mm gold and 3 mm glassy carbon electrodes showed similar results.

Since the deposited Si largely insulates the underlying Pt, one can estimate the extent and nature of the coverage by determining the CV or chronoamperometry of a soluble reversible redox species, e.g. ferrocene, at the bare and progressively covered electrode, in a method analogous to that used to study the deposition of a polymer on an electrode [15]. To study the proposed growth stages, different amounts of Si (Si–H) were deposited on a 2 mm Pt electrode using chronocoulometry and the electrode was removed and the

extent of coverage found from the CV of the ferrocene redox reaction (Fig. 6c). A clean 2 mm Pt electrode showed reversible redox peaks for ferrocene with $\Delta E = 81$ mV (a in Fig. 6c); the large peak splitting is attributable to uncompensated resistance. Pt electrodes with Si deposits (1 and 10 ms deposition time, corresponding to region A in the chronoamperogram in Fig. 6a) showed reversible redox peaks for ferrocene with an increase in ΔE_p (96 and 107 mV, respectively) and a decrease in charging current (b and c in Fig. 6c) but with a similar peak current (i_{pa}) as in a. A Pt electrode with a Si deposit (250 ms deposition time, corresponding to region B in Fig. 6a) showed a wave for ferrocene resembling a steady state response (d in Fig. 6c) smaller than i_{pa} in a. Pt electrodes with Si deposits (1, 3, and 5 s deposition times, corresponding to regions C and D in Fig. 6a) showed an oxidation wave for ferrocene with a current of about 5–10% of that with a clean Pt electrode (e, f, g in Fig. 6c). Characteristic features of a Pt electrode with a Si deposit for the ferrocene redox reaction are a shift of E_p to more positive values, a larger ΔE_p, and smaller charging current. Pt electrodes with Si deposits thus showed characteristic behavior depending on the amount of Si deposited and the results correspond well with the regions of Si growth observed in the chronoamperogram. Experiments with a 3 mm glassy carbon electrode showed similar results. Chronoamperograms of 1 mM ferrocene with Si-deposited Pt electrodes showed similar behavior. A clean Pt electrode showed Cottrell behavior for ferrocene, while Si-deposited Pt electrodes showed a decrease in slopes of current transients (i vs. $t^{-1/2}$).

A chronoamperogram obtained from a solution of SiCl$_4$ showed a similar current transient curve (Fig. 7a) as the SiHCl$_3$ system. The rise in current after the steady state current region is possibly due to IR drop in the solution or perhaps a nucleation phenomenon. Chronoamperometry experiments with positive feedback IR compensation resulted in the absence of current rise after the steady state current region in one case but in other cases, resulted in a distorted current transient curve. Chronoamperograms obtained from a 25 mM SiCl$_4$ solution using a 2 mm Pt electrode at different overpotentials (-1.73, -1.80, -1.90, -2.00, and -2.10 V) showed different rates of Si growth and inhibition times and a chronoamperogram obtained from a 100 mM SiCl$_4$ solution (overpotential: -2.10 V) showed a steady state current region followed by growth inhibition and slow growth region. Cyclic voltammetry studies of the ferrocene redox reaction with Si-deposited Pt electrodes showed irreproducible results because of non-uniform Si deposition on Pt (as seen in bulk electrodeposition, Fig. 1c). A chronoamperogram obtained using a 3 mm glassy carbon electrode from a SiCl$_4$ solution is shown in Fig. 7b and cyclic voltammetry studies of the ferrocene redox reaction with Si deposited on glassy carbon electrodes indicated that the growth could be described as occurring via four stages (1) nucleation and localized growth, (2) growth in between islands, (3) growth inhibition and (4) slow growth.

Cyclic voltammetry of anthraquinone and ferrocene showed a reduction wave for anthraquinone and an oxidation wave for ferrocene before deposition but essentially complete suppression of both waves after deposition (Fig. 7c). Irradiation of the deposited Si films with a quartz halogen lamp showed no photoactivity as might be expected if n- or p-type Si was deposited. When a smaller
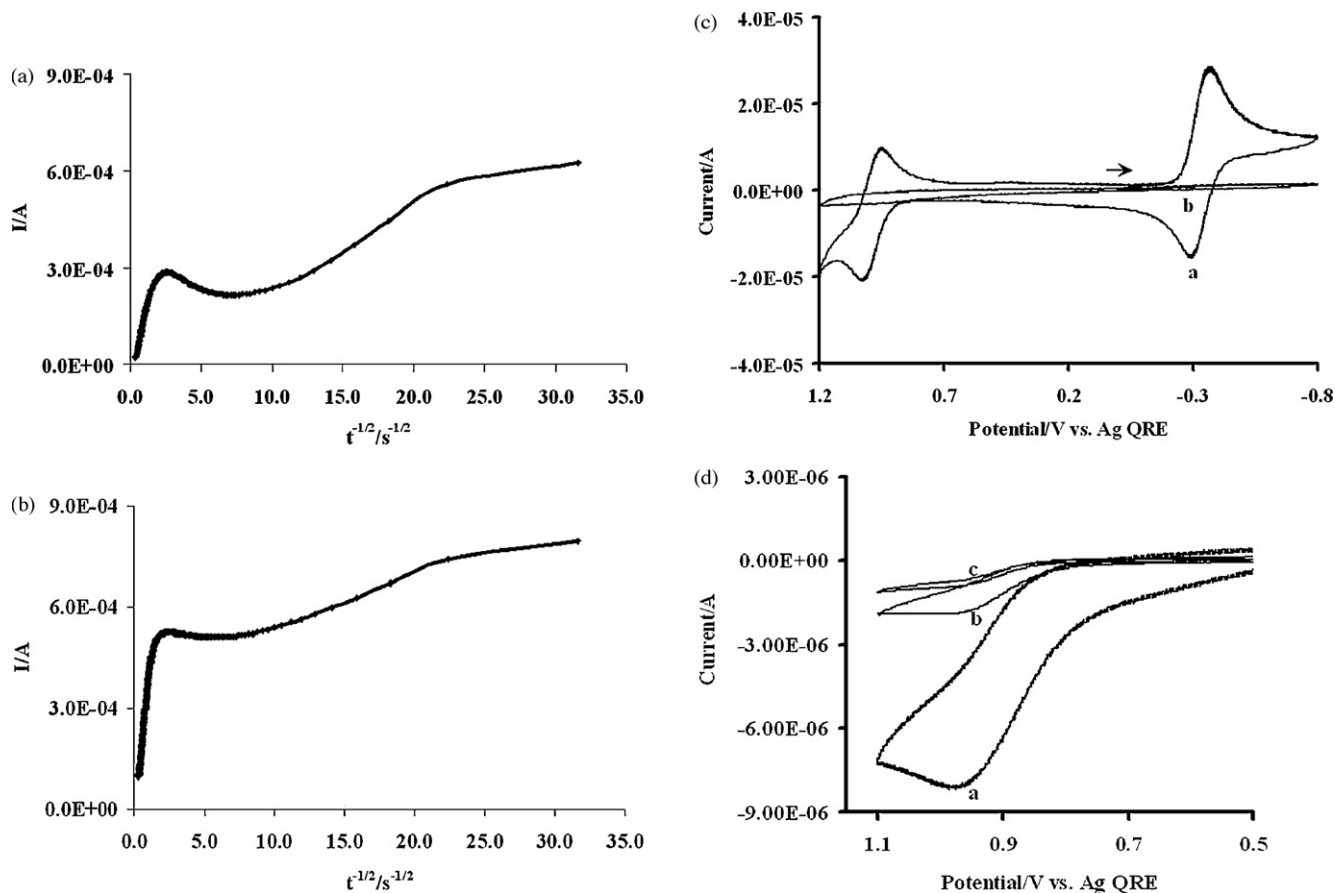

Fig. 7. (a) Chronoamperogram of 15 mM SiCl$_4$ in 0.1 M TBACl and CH$_3$CN. W.E. 2 mm Pt. $E_i = -1.0$ V vs. Ag QRE, $E_f = -1.64$ V vs. Ag QRE. (b) Chronoamperogram of 15 mM SiCl$_4$ in 0.1 M TBACl and CH$_3$CN. W.E. 3 mm GC. $E_i = -1.0$ V vs. Ag QRE, $E_f = -1.73$ V vs. Ag QRE. (c) Cyclic voltammograms of 1 mM anthraquinone and 1 mM ferrocene in 0.1 M TBACl and CH$_3$CN: a, 2 mm Pt electrode; b, Si-deposited Pt electrode (42452 μC/cm^2); (d) Cyclic voltammograms of 1 mM ferrocene in 0.1 M TBACl and CH$_3$CN using a Si-deposited Pt electrode (10445 μC/cm^2): a, 0.2 V/s; b, 0.020 V/s; c, 0.005 V/s.

amount of Si ($10\,mC/cm^2$) was deposited on a Pt electrode, a scan rate (ν) dependent response for the ferrocene redox reaction could be observed. At $\nu = 0.2\,V/s$, a peak-shaped response was observed for ferrocene (a in Fig. 7d). At smaller ν (0.020, 0.005 V/s), steady state responses were seen, indicating that the electrode was behaving as a group of ultramicroelectrodes (b and c in Fig. 7d). The above result confirms the presence of small defects in the deposited Si films.

4. Discussion

Previous reports and the current study indicate that while Si films ranging in thickness (0.2–$3\,\mu m$) can be electrodeposited, the quality of the deposits is poor because of stressed growth and incorporation of species from the supporting electrolyte and solvent. The stressed growth occurs after a layer of Si ($\sim 2\,nm$) is electrodeposited on the metal substrate which acts as an insulator and further growth occurs by a combination of structural rearrangement and diffusion of the Si precursor through the defects. By processing the Si deposits after electrodeposition it might be possible to remove bath impurities and annealing generally results in relatively stable films with lower impurities [12]. Deposition of nanoscale Si [16] and metal-induced crystallization of amorphous Si to form polycrystalline Si might be of interest.

5. Conclusions

Si was electrodeposited on Ni, Ag and GC substrates from baths containing (1) $0.3\,M$ $SiCl_4$, $0.1\,M$ TBACl and CH_3CN and (2) $0.3\,M$ $SiHCl_3$, $0.1\,M$ TBACl and THF. The deposited amorphous films contained C, N and Cl impurities and oxidized on contact with air. XPS characterization of a deposit with minimum exposure to air shows that pure Si (2p, 99.5 eV) is electrodeposited. Annealing of deposits after electrodeposition under an argon atmosphere at temperatures ranging from 350 to 800 °C generally showed a reduced presence of oxygen and lower concentrations of C, N and Cl. Annealing a deposit at 350 °C for 30 min in the presence of a Sn/Pb metal mixture helped to crystallize the Si and results in weak p-type photoactivity of the sample. Finally, cyclic voltammetry and chronoamperometry studies suggest that the Si growth occurs in four stages (1) nucleation and localized growth, (2) growth between the islands, (3) growth inhibition and (4) a slow growth stage, with growth inhibited after a layer ($\sim 2\,nm$) of Si is deposited on the substrate. None of the films showed the desired photoelectrochemical behavior, however.

References

[1] G. Beaucarne, A. Slaoui, in: J. Poortmans, V. Arkhipov (Eds.), Thin Film Solar Cells: Fabrication, Characterization and Applications, John Wiley & Sons, West Sussex, 2006, p. 123.
[2] M. Zeman, in: J. Poortmans, V. Arkhipov (Eds.), Thin Film Solar Cells: Fabrication, Characterization and Applications, John Wiley & Sons, West Sussex, 2006, p. 173.
[3] M. Paunovic, M. Schlesinger, Fundamentals of Electrochemical Deposition, 2nd ed., Wiley-Interscience, Hoboken, NJ, 2006.
[4] R.K. Pandey, S.N. Sahu, S. Chandra, Handbook of Semiconductor Electrodeposition, Marcel-Dekker, New York, NY, 1996, p. 193.
[5] M. Estela Calixto, K.D. Dobson, B.E. McCandless, R.W. Birkmire, J. Electrochem. Soc. 153 (2006) G521.
[6] D. Lincot, J.F. Guillemoles, S. Taunier, D. Guimard, J. Sicx-Kurdi, A. Chaumont, O. Roussel, O. Ramdani, C. Hubert, J.P. Fauvarque, N. Bodereau, L. Parissi, P. Panheleux, P. Fanouillere, N. Naghavi, P.P. Grand, M. Benfarah, P. Mogensen, O. Kerrec, Solar Energy 77 (2004) 725.
[7] A.K. Agrawal, A.E. Austin, J. Electrochem. Soc. 128 (1981) 2292.
[8] J. Gobet, H. Tannenberger, J. Electrochem. Soc. 135 (1988) 109.
[9] J.P. Nicholson, J. Electrochem. Soc. 152 (2005) C795.
[10] Y. Nishimura, Y. Fukunaka, Electrochim. Acta 53 (2007) 111.
[11] J.S. Pan, A.T.S. Wee, C.H.A. Huan, H.S. Tan, K.L. Tan, J. Appl. Phys. 79 (1996) 2934.
[12] E.R. Bucker, J.A. Amick, U.S. Pat. No. 4,192,720 (1980).
[13] W. Knaepen, C. Detavernier, R.L. Van Meirhaeghe, J. Jordan Sweet, C. Lavoie, Thin Solid Films 516 (2008) 4946.
[14] S.W. Lee, S.K. Joo, U.S. Pat. No. 6,692,996 (2004).
[15] P. Peerce, A.J. Bard, J. Electroanal. Chem. 112 (1980) 97.
[16] J. Mallet, M. Molinari, F. Martineau, F. Delavoie, P. Fricoteaux, M. Troyon, Nanoletters 8 (2008) 3468.